

Near Band-Edge Optical Excitation Leading to Catastrophic Ionization and Electron–Hole Liquid in Room-Temperature Monolayer MoS₂

Robert Younts, Alexander Bataller, Hossein Ardekani, Yiling Yu, Linyou Cao, and Kenan Gundogdu*

Atomically thin materials exhibit exotic electronic and optical properties. Strong many-body interactions from the reduced dielectric environment lead to electronic phases that drastically change conductivity and optical response. For example, these many-body interactions can give rise to the formation of collective states such as Mott metal–insulator transitions, electron–hole liquids and plasmas, and excitonic condensates, which typically occur at cryogenic temperatures and high excitation densities. Herein, it is demonstrated that in monolayer MoS₂ at room temperature, a low-density (10^{10} cm^{-2}) excitonic gas is formed with continuous wave (CW) below-gap optical excitation. A slight increase in the excitation fluence triggers a nanosecond phase transition into a dense electron–hole liquid state with three orders of magnitude higher carrier density. This investigation suggests that while the material is in equilibrium with the CW excitation at the threshold fluence, thermomechanical expansion combined with continuous renormalization of the band gap leads to a sudden increase of optical absorption, which initiates runaway exciton ionization and the formation of a high density electron–hole plasma. Such abrupt changes in the excitation density and carrier population can be the basis of unprecedented applications based on 2D materials.


1. Introduction

Optical excitations in semiconductors exhibit many-body interactions that drastically alter the electronic and optical properties. At low excitation, these many body interactions lead

Dr. R. Younts, Dr. A. Bataller, H. Ardekani, Prof. L. Cao, Prof. K. Gundogdu
Department of Physics
North Carolina State University
Raleigh, NC 27695, USA
E-mail: kgundog@ncsu.edu

Dr. Y. Yu, Prof. L. Cao
Department of Materials Science and Engineering
North Carolina State University
Raleigh, NC 27695, USA

Prof. L. Cao
Department of Electrical and Computer Engineering
North Carolina State University
Raleigh, NC 27695, USA

 The ORCID identification number(s) for the author(s) of this article can be found under <https://doi.org/10.1002/pssb.201900223>.

DOI: 10.1002/pssb.201900223

to excitons,^[1] trions,^[2] and biexcitons^[3] that are formed from few quasiparticle correlations. At high excitation fluence in certain semiconductors, collective interactions of these excitations lead to macroscopic states, such as electron–hole liquid and plasma.^[4,5] The formation of these collective states requires critical conditions such as low temperature and high excitation density. Hence experiments have to be under cryogenic conditions and laser illumination above the band gap.^[4,5] Recent work on 2D MoS₂ showed that it is possible to create an EHL phase in 2D transition metal dichalcogenides (TMDs) at room temperature.^[6] Here we show that it is possible to excite electron–hole liquid (EHL) and dense electron–hole plasma (EHP) phases in 2D MoS₂ with the laser wavelength tuned slightly below the band gap of the material. While reaching a critical excitation density for the EHL phase transition is not possible with below-gap excitation in conventional semiconductors, such a phase transition is possible in 2D

materials because the thermal heating can significantly shift the absorption.

2. Results

Figure 1a shows the absorption spectra (red line) and photoluminescence (PL, blue line) of free-standing monolayer MoS₂. The two spectral features located at 1.89 and 2.04 eV are the A and B excitons, respectively, which are the two spin–split optical transitions in the K-valley.^[1] At room temperature and moderate photon fluence, optical excitation result in tightly bound excitons.^[7] Figure 1b shows the PL progression with increasing power when the material is excited using below-gap photons (1.81 eV). At relatively low fluence, the PL is weak due to low absorption and is dominated by A-exciton recombination. The weak PL at low fluence is only observable in Figure 1b inset, where the intensity is multiplied by 100. The PL at this low fluence (from 0.6 to 1.2 mW) exhibits a linear dependence with power, which indicates a low-density exciton regime. The linear dependence of the PL suggests that it does not originate

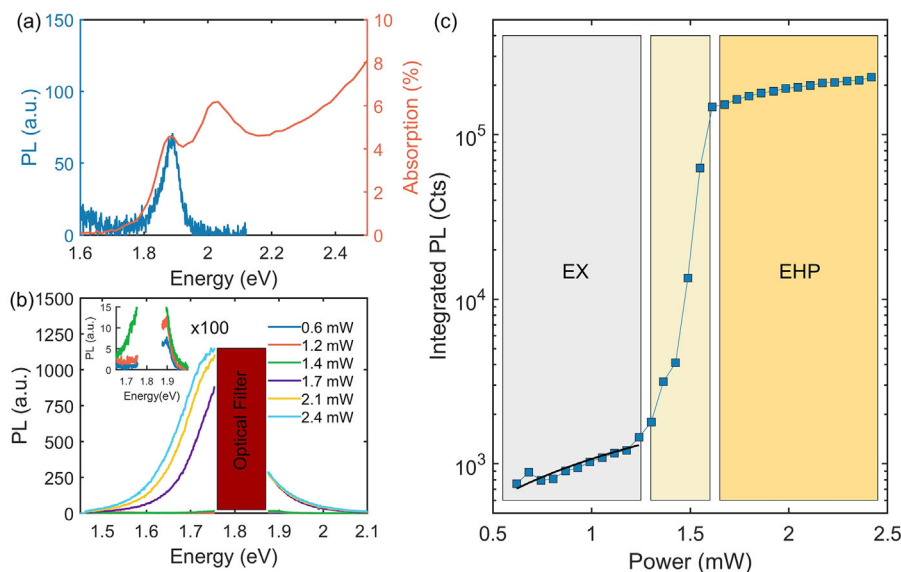


Figure 1. a) The absorption (red) and photoluminescence (blue) of free-standing monolayer MoS₂. The photoluminescence was excited with above-gap light (2.32 eV) under low fluence. b) The evolution of the PL spectra measured at different powers for the below-gap excitation (1.81 eV). The spectral gap in the photoluminescence corresponds to the optical filter used to block the excitation wavelength. The PL in that region is not measured. c) Integrated intensity at different excitation powers. The black line from 0.6 to 1.2 mW is a linear fit to the integrated PL with respect to power.

from nonlinear multiphoton excitation, but rather due to excitation of defect states below the band edge. It is likely that a small population of these excitations can thermalize and contribute to the PL. The PL intensity experiences a dramatic increase beyond a laser power threshold of 1.35 mW (51 kW cm⁻²). Astonishingly, a mere 10% increase in photoexcitation at the threshold results in >100-fold increase in integrated PL in Figure 1c. Compared to the exciton emission at low fluence above the threshold, the spectrum is red-shifted by 70 meV and has a much broader line width (≈175 meV). This new PL spectral line shape is identical (width, peak energy, and intensity) to the PL from dense EHP and EHL states created with above-gap excitation, as we have reported elsewhere,^[6,8] and also in Figure S1, Supporting Information. We conclude this sharp threshold at elevated photoexcitation originates from a phase transition of excitons into EHL.

The ionization of excitons and subsequent EHL phase transition with below-gap optical excitation is quite surprising, as the process requires high exciton densities.^[9–11] The electrostatic model of plasma formation requires high excitation density for exciton–exciton screening. When the Debye–Hückel screening length becomes comparable to the distance between excitons, the binding energy vanishes and excitons ionize.^[10,12] This effect is described as “ionization catastrophe” in the literature and has been observed in several semiconductors.^[10–14] Recent efforts in 2D materials, specifically MoS₂, WS₂, and MoTe₂ have revealed such a phase transition under intense photoexcitation.^[6,15,16] In these observations, ultrathin semiconductors were excited using photon energies higher than the band gap, which created a sufficiently dense population of excitons. Astonishingly, the below-gap photoexcitation that was utilized in this study triggered ionization of excitons and a phase transition into the EHL phase.

In order to compare the critical exciton density for above and below gap excitation conditions, we performed an experiment using 532 nm laser photoexcitation (above-gap) and measured the threshold power for the plasma phase transition and calculated the required exciton density for phase transition with the above-gap excitation (see Supporting Information). For steady-state photoexcitation, the rate of charge generation and recombination must be in balance, i.e., $G - k_r N_{EX} - k_{EEA} (N_{EX})^2 = 0$. In this equation, G is the exciton generation rate that depends on absorption coefficient of 6% (at 532 nm) and the incident laser power, k_r is the exciton recombination lifetime of 10⁻⁹ s,^[17] and k_{EEA} is the exciton–exciton annihilation time for suspended MoS₂ of 0.1 cm² s⁻¹.^[18] Using this equation at different photoexcitation powers we estimate ≈10¹¹ cm⁻² excitons are needed for complete ionization for above-gap photoexcitation (see Supporting Information). The equilibrium exciton density was calculated for the low power, above-gap PL measurements from Figure S1, Supporting Information. Using the correlation between peak PL emission and exciton density for those low power, above-gap PL measurements (see Figure S2, Supporting Information), we estimate that the below-gap photoexcitation (1.81 eV) with 1.35 mW (51 kW cm⁻²) of laser power creates ≈10¹⁰ cm⁻² excitons. In the below gap case, the exciton density is an order of magnitude lower than what is required for ionization (see Supporting Information).

To investigate the mechanism that leads to photoionization at low exciton density, we performed time-resolved PL (TR-PL) and time-resolved differential transmission spectroscopy (TR-DTS) experiments and compared the carrier dynamics for below-gap and above-gap photoexcitation. During these time-resolved experiments, we observed that when below-gap excitation is used, the plasma emission is only observed if the excitation is longer than 100 ns. Moreover, the necessary exposure time for

plasma formation depends on the particular MoS₂ flake, which can range from hundreds of nanoseconds to upwards of 1 s. In stark contrast to the below-gap excitation, the above-gap excitation generates plasma abruptly, even with femtosecond excitation,^[15] and does not exhibit a significant variation in the threshold power.

Figure 2 shows the PL evolution under pulsed excitation measured via time-correlated single photon counting. Laser pulses with a temporal width of 500 and 2000 ns are used for above and below gap excitation, respectively. In both experiments, we measured the PL time evolution at the A-exciton (1.89 eV) and the EHP (1.72 eV) energies. For both, above-gap and below-gap excitations, the peak photoexcitation intensity was chosen to create the same final equilibrium EHP state measured by CW-PL experiments (see Figure S3, Supporting Information). It is important to note that during the time evolution of the PL, the 1.89 eV emission is from exciton recombination, however, at later delays once EHP forms, the PL at 1.89 eV is no longer from the A exciton state, but rather from the broad tail of the EHP emission.

For above-gap excitation, the exciton PL emission (1.89 eV) grows with time and reaches a maximum value within the first 50 ns of the laser exposure, and then decays as the EHP emission (1.72 eV) grows. PL from the EHP state reaches equilibrium within 100 ns. In contrast, when the same MoS₂ flake excited using below-gap photons, the exciton emission is 30× weaker, and exhibits a slight rise for 500 ns, after which it remains stable. The EHP emission does not begin until 300 ns of laser exposure. After 300 ns, the EHP emission increases sharply, and then stabilizes at 500 ns. Curiously, the exciton emission prior to plasma emission is over an order of magnitude weaker for below-gap excitation than for the above-gap excitation, suggesting that a low exciton density can somehow lead to ionization.

The PL experiment measures population only if the photoexcitations radiatively recombine. In addition, PL lifetime measurements are specific to a single emission wavelength. During the transition, the PL emission exhibits dynamic spectral evolution, and therefore the tr-PL measurements at a specific

wavelength do not reveal exciton population. To probe the carrier population build up during the long wait time prior to EHP formation, we performed TR-DTS, which measures population kinetics even when there is no radiative recombination. **Figure 3** shows the dense EHP phase evolution measured using TR-DTS on a MoS₂ flake that exhibits a longer phase transition time than the flake used in PL measurements in Figure 2. The TR-DTS for above-gap and below-gap photoexcitation are shown in Figure 3a and b for a spectral region covering the entire exciton and plasma response. In Figure 3a and b, the spectral features located at 1.9 and 2.02 eV are attributed to A and B excitons, respectively.^[3] The feature at 1.8 eV is attributed to the absorption of the plasma states.^[6] The A-exciton (1.90 eV) and EHP (1.80 eV) dynamics for both, above-gap and below-gap photoexcitation are shown in Figure 3c and d, respectively. The evolutions of these spectral features effected by both population and also temperature-induced shifts in the absorption. Similar to the TR-PL experiments for above-gap excitation, the exciton and EHP features form immediately with the start of the laser pulse. In stark contrast, the below gap excitation has almost no differential transmission at EHP frequencies for 1.8 μs. The evolution of the differential transmission at the exciton energies is rather interesting. For the first 300 ns, the differential transmission in the exciton feature increases to 0.13% with a relatively fast rate. The exciton differential transmission then slowly increases to 0.2% in 1.5 μs. Only when the 0.2% exciton differential transmission is reached, the plasma differential transmission signal rises abruptly (Figure 3d). Interestingly, the exciton signals are the same for both, above-gap and below-gap conditions at the plasma formation threshold. In other words, although PL emission is nearly absent before plasma formation for below gap photoexcitation, the differential transmission experimental data suggest photoexcitation density builds up over the time of the exposure and lead to ionization, when it reaches similar density as above gap excitation.

The results of the TR-PL and TR-DTS experiments indicate that the plasma formation with below gap excitation is a multistep process. Just below the threshold power, there is relatively a small density ($\approx 10^{10}$ cm⁻²) of excitations created by

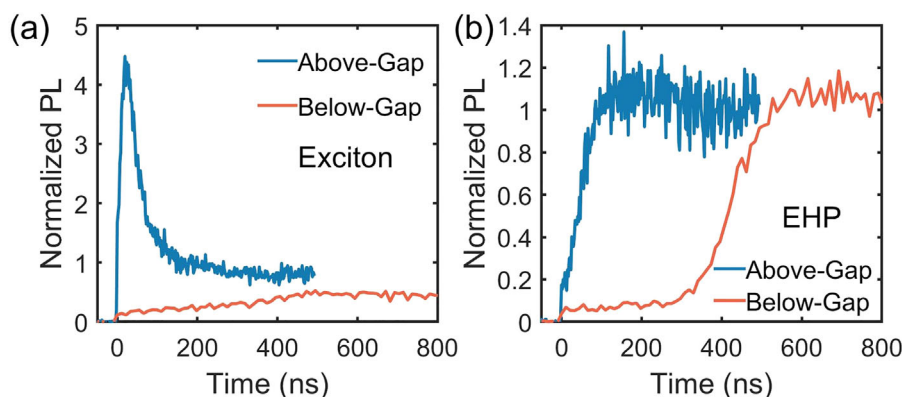


Figure 2. a) TR-PL at the exciton energy (1.89 eV) for above-gap (1.95 eV/1.9 mW) and below-gap (1.81 eV/3.3 mW) photoexcitation. Due to the photoexcitation energies and corresponding filters used in the measurement, the exciton emission was measured at 1.84 and 1.89 eV for above and below-gap photoexcitation, respectively. b) TR-PL at the EHP energy (1.72 eV) for above and below-gap photoexcitation.

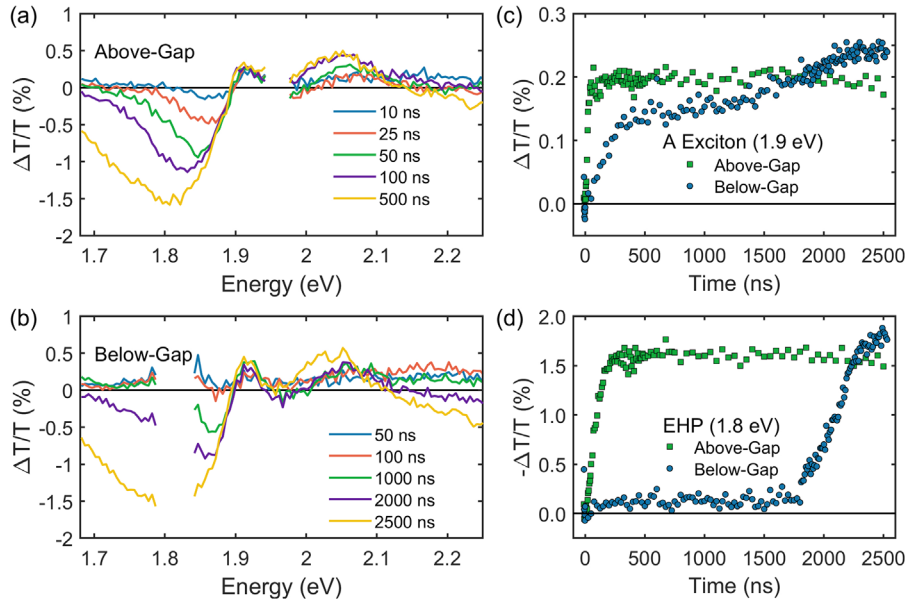


Figure 3. Time-resolved differential transmission spectroscopy at various time delays for a) above-gap (1.95 eV/1.4 mW) and b) below-gap (1.81 eV/2.5 mW) photoexcitation at intensities above the ionization threshold. c) A-exciton and d) EHP transmission dynamics for above and below-gap photoexcitation.

the below gap excitation due to absorption into the low-energy exciton tail and in-gap defect states.^[19] Since the exciton lifetime in MoS₂ is ≈ 1 ns,^[17] the excited-state population should be equilibrated in a few nanoseconds for steady-state photoexcitation. However, the threshold is reached with only 10% increase in the laser power and only if the laser exposure is long enough. In this case, the TR-PL and TR-DTS dynamics initially show a relatively small density. However, it is not in equilibrium. In other words, the PL shows a slight increase and the TR-DTS exhibits a large increase, which indicates a change in the excitation density created in the material over hundreds of ns time scale. During that time scale, the most probable change in the material is thermal heating and resulting expansion of the material due to low thermal conductivity and the relatively long time of the laser exposure.^[20] A direct consequence of photo-thermal lattice expansion is a reduction in the band gap.^[21] Band gap reduction produces an increase in the absorption coefficient at the band edge, which leads to a rise in the photoexcitation density. The resulting absorption increase acts as a positive feedback for increasing the exciton density. This manifests as a growth in both the exciton differential transmission signal and photoluminescence. During the first 1.8 μ s, the temperature increases and the absorption redshifts. However, the effect is most dramatic in the first 300 ns because the initial absorption of the below gap excitation is negligible, where even a small shift causes a dramatic increase in the excitation density. Once the A-exciton differential transmission level of 0.2% is reached, exciton ionization occurs. One of the surprising observations is that although the differential transmission signal reaches the same level for both, above-gap and below-gap excitation experiments, in the former case exciton emission is strong, whereas in the latter it is very weak. In a sense, there is a population of “dark” excitations that accumulates over time for the below gap case.

To investigate why an increased excitation population does not lead to intense excitonic PL prior to plasma generation, we performed Raman scattering experiments. Raman measurements provide information about the temperature and the strain build up in the material due to lattice expansion.^[22] By measuring the lattice expansion, we can infer changes in the electron band structure. In Figure S4, Supporting Information, we measured the Stokes and anti-Stokes Raman scattering peaks for the A₁ and E' modes, which provides a localized temperature measurement (see Supporting Information). As previously reported,^[22] the peak position of the E' mode is a strong indicator of lattice expansion. **Figure 4** shows the monolayer temperature, E' peak position, and relative lattice expansion as a function of below-gap excitation power. All measurements are performed at room temperature. At excitation levels below the threshold, the temperature is about 380 K. When the power is

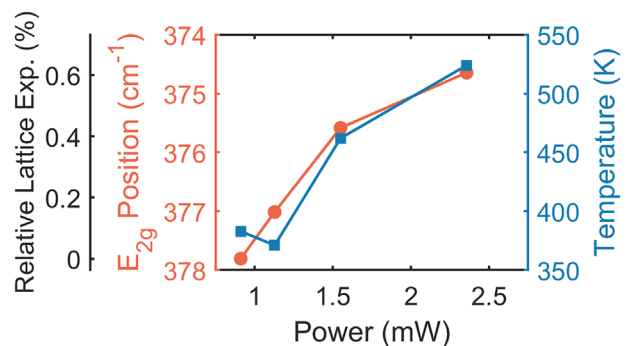


Figure 4. Monolayer MoS₂ Raman mode E' position/relative lattice expansion (left axis) and temperature (right axis) as a function of laser power for the below-gap excitation.

increased to 2.4 mW, catastrophic ionization takes place, and the temperature increases to 460 K. The material lattice expands with increasing excitation, which is consistent with a temperature increase from photothermal heating. As reported elsewhere, lattice expansion in MoS₂ leads to a direct-to-indirect band transformation, where the conduction band in the K-valley and valance band in the Γ -valley form the lowest electron and hole levels, respectively.^[8] As a result, the exciton population increase does not lead to a substantial PL increase.

3. Discussion

Based on our steady-state and TR-PL, TR-DTS, and Raman experiments, we now present a model that describes this unusual ionization process as detailed in **Figure 5**. As inferred by the relative exciton luminescence and the equilibrium exciton density, the absorption coefficient at 1.81 eV is $\ll 1\%$, and therefore the equilibrium exciton density of $\approx 10^{10} \text{ cm}^{-2}$ is well below the plasma formation threshold (see Supporting Information). However, continuous optical excitation generates a temperature increase as observed by Raman measurements. As the temperature increases, the below-gap optical absorption also increases due to thermal-induced band gap reduction. At high temperature, the lattice expansion further changes the electronic band structure toward an indirect gap. As a result, a high exciton density is created without significant PL emission. At high enough exciton densities, band gap renormalization leads to plasma generation. The large variation in the laser power and the laser exposure time to induce ionization with the below-gap excitation arises from the need for a specific thermal-induced

lattice expansion to create the band structure conducive to plasma formation. The dependence of band edge absorption on defect density, and its variance across samples may be responsible for the change in the photothermal dynamics and therefore the laser power and exposure time needed for ionization.

4. Conclusion

In summary, we showed that it is possible to excite a high-density electron-hole plasma state using a below-gap excitation in monolayer MoS₂. While at first the optical photoexcitation creates an order of magnitude smaller exciton density compared to the plasma phase transition, shifts in the absorption spectra and changes in the electronic band structure due to lattice expansion from material heating leads to an increased exciton population and runaway ionization. The result is a sudden 1000-fold increase in the carrier density and electron-hole plasma state with 100-fold increase in total luminescence. The sharp change in carrier density from an insulating exciton gas (10^{10} cm^{-2}), to a conductive electron-hole plasma (10^{13} cm^{-2}) along with the change in luminescence properties makes monolayer MoS₂ a potential candidate for novel, high-density, energy dense, switchable photonic devices.

5. Experimental Section

Sample Preparation: Quartz substrates were patterned with micron-scale holes using standard photolithography and dry etching for the fabrication of free-standing monolayers. The monolayer materials were

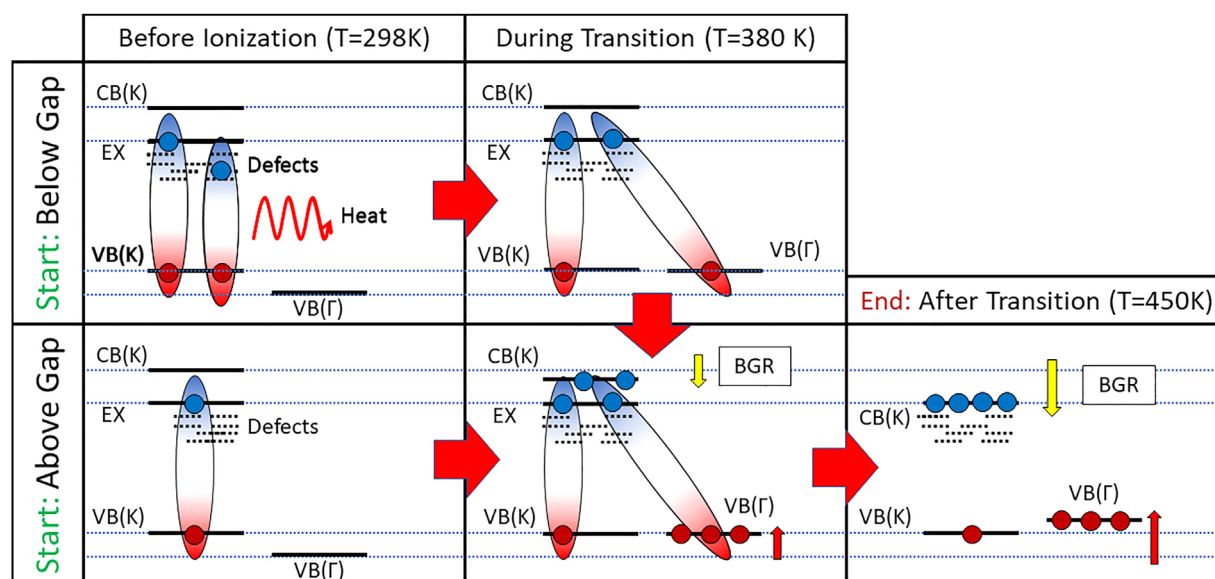


Figure 5. Diagrammatic representation for the ionization process of excitons into free carriers with both below-gap and above-gap excitation. For below-gap excitation, Step 1: At room temperature with a dilute exciton gas, the band structure is unperturbed with both free and bound excitations present. Step 2: Photothermal expansion from nonradiative recombination of both bound and free carriers shifts the Γ VB to be nearly isoenergetic with the K-point VB. Step 3: Larger exciton populations in the indirect state drive charge screening and ionization. Step 4: Ionization continues and photothermal expansion continues until a dense plasma is formed in the Γ valence band and K conduction band. For above-gap excitation, Step 1: At room temperature a dense exciton gas is present, causing photothermal expansion and BGR leading to Steps 3 and 4 for the below-gap case.

obtained from 2DLayer, which were grown on sapphire substrates using chemical vapor deposition.^[23] They were then transferred to the patterned quartz substrates using a surface-energy assisted transfer method.^[24] The transfer was done by spin-coating a solution of 9 g of polystyrene (PS, MW = 280 kg mol⁻¹) dissolved in 100 mL of toluene at 3000 rpm for 60 s on the as-grown monolayers, which was followed by a 80–90 Celsius bake for 1 h. A water droplet was dropped on the PS/monolayer to lift it from the substrate. The PS/monolayer assembly was then transferred to the patterned quartz substrate. The sample was baked at 80 Celsius for 1 h and then 30 min at 150 Celsius with a toluene rinse to remove the PS.

Steady State Photoluminescence: Steady state photoluminescence measurements were performed using a 685 nm Coherent OBIS laser for below-gap photoexcitation and a 532 nm Coherent Verdi laser for above-gap photoexcitation. Both lasers were focused to <1.5 μm FWHM through a 50× microscope objective onto free-standing MoS₂. PL was collected through the same objective and spectrally resolved on a CCD camera. A 30 nm wide notch filter centered at 685 nm was used to block the below-gap photoexcitation, whereas a 550 nm long-pass filter was used to block the above-gap photoexcitation.

Since the notch filter also blocks PL in that same region from reaching the detector, additional numerical analysis was needed to calculate the spectral position, width, and integrated PL. This was done by first interpolating the missing PL spectrum with a third-order polynomial fit. The spectral width FWHM (e⁻²) was determined by finding the energies where the maximum PL intensity decreased by 1/e². The spectral center was then determined as half-way between those energies. The integrated PL was then calculated as the sum of the emission including the interpolated region.

Time-Resolved Photoluminescence: Time-resolved photoluminescence measurements were performed with either a 685 or 635 nm Coherent OBIS laser for below-gap and above-gap photoexcitation, respectively. Both lasers were focused to <1.5 μm FWHM through a 50× microscope objective onto free-standing MoS₂. PL was collected through the same objective and spectrally resolved with a monochromator before being collected by a photomultiplier tube (PMT). A delay generator was used to pulse the photoexcitation laser at 100 kHz with an arbitrary pulse width. Time correlation was completed by measuring the time between the laser pulse and PL emission collected by the PMT by means of a time-to-amplitude converter. The PL counts from the PMT were then histogrammed based on their collection time.

Time-Resolved Differential Transmission Spectroscopy: Time-resolved differential transmission spectroscopy measurements were performed using the same Coherent OBIS lasers as the TR-PL measurements as the pump source. The probe was generated using a broadband white-light continuum generated from an amplified femtosecond laser (800 nm, 10 kHz rep. rate) focused through a sapphire plate. The OBIS laser was synced with the output of the femtosecond amplifier by using a delay generator and triggered at 5 kHz. The delay generator controlled the time between pump and probe on the sample. Both the pump and probe lasers were focused collinearly through the 50× microscope objective. The transmitted probe was collected and collimated through a matching objective and then passed to the Princeton Instruments Fergi spectrometer. The Fergi spectrometer was triggered to capture a single shot of the probe spectrum a 10 kHz. Every other shot collected by the Fergi contained the transmission when the pump illuminated the sample. The difference in transmission, pump on versus pump off, was calculated by subtractive every other spectrum collected by the Fergi and then divided by the average probe only spectrum to get a relative differential transmission spectrum.

Raman Spectroscopy: Raman spectroscopy measurements were performed using the 532 nm Coherent Verdi laser and the 685 nm Coherent OBIS laser. The 532 nm laser was kept at a constant low power <0.1 mW and focused through the 50× microscope objective to a spot with <1.5 μm FWHM. Reflected light was collected through the same objective and spectrally resolved with a CCD camera. A 10 nm notch filter was used to block the fundamental laser while allowing the transmission of Stokes and anti-Stokes Raman scattered light. An additional 685 nm

laser was focused to the same spot as the 532 nm laser to excite monolayer MoS₂ below-gap. The power of the 685 nm laser was swept through the EHP transition while measuring Raman scattering with the 532 nm laser.

Supporting Information

Supporting Information is available from the Wiley Online Library or from the author.

Authors' Contributions

K.G. and R.Y. designed the research. L.C. and Y.Y. provided the samples. R.Y., A.B., and H.A. performed the optical and Raman measurements. R.Y. analyzed the experimental data. R.Y. drafted the manuscript with K.G. and received contributions from all authors.

Acknowledgment

The authors acknowledge funding from ARO grant # W911NF-17-1-0483 and NSF DMR-1709934.

Conflict of Interest

The authors declare no conflict of interest.

Keywords

2D materials, electron–hole liquid, MoS₂, Mott transition

Received: April 24, 2019

Revised: May 16, 2019

Published online:

- [1] K. F. Mak, C. Lee, J. Hone, J. Shan, T. F. Heinz, *Phys. Rev. Lett.* **2010**, *105*, 136805.
- [2] K. F. Mak, K. He, C. Lee, G. H. Lee, J. Hone, T. F. Heinz, J. Shan, *Nat. Mater.* **2013**, *12*, 207.
- [3] C. Mai, A. Barrette, Y. Yu, Y. G. Semenov, K. W. Kim, L. Cao, K. Gundogdu, *Nano Lett.* **2013**, *14*, 202.
- [4] C. D. Jeffries, L. V. Keldysh (Eds.), *Electron–Hole Droplets in Semiconductors*, Modern problems in condensed matter sciences Vol. 6, North Holland Publication Company, Amsterdam **1983**.
- [5] C. D. Jeffries, *Science* **1975**, *189*, 955.
- [6] Y. Yu, A. Bataller, R. Younts, Y. Yu, G. Li, A. A. Puzetzk, D. B. Geohegan, K. Gundogdu, L. Cao, *Room-Temperature Electron–Hole Liquid in Monolayer MoS₂*, **2017**, arXiv preprint arXiv:1710.09538.
- [7] a) Y. Yu, Y. Yu, Y. Cai, W. Li, A. Gurarlan, H. Peelaers, D. E. Aspnes, C. G. Van de Walle, N. V. Nguyen, Y.-W. Zhang, *Sci. Rep.* **2015**, *5*, 16996; b) L. Wang, A. Kutana, B. I. Yakobson, *Annalen der Physik* **2014**, *526*, L7; c) A. Klots, A. Newaz, B. Wang, D. Prasai, H. Krzyzanowska, J. Lin, D. Caudel, N. Ghimire, J. Yan, B. Ivanov, *Sci. Rep.* **2014**, *4*, 6608.
- [8] A. W. Bataller, R. Younts, A. Rustagi, Y. Yu, H. Ardekani, A. Kemper, L. Cao, K. Gundogdu, *Nano Lett.* **2019**, *19*, 1104.
- [9] N. Mott, *Rev. Modern Phys.* **1968**, *40*, 677.

- [10] J. Shah, M. Combescot, A. Dayem, *Phys. Rev. Lett.* **1977**, *38*, 1497.
- [11] E. J. Sie, A. J. Frenzel, Y.-H. Lee, J. Kong, N. Gedik, *Phys. Rev. B* **2015**, *92*, 125417.
- [12] D. Snoke, *Solid State Commun.* **2008**, *146*, 73.
- [13] R. Shimano, M. Nagai, K. Horiuchi, M. Kuwata-Gonokami, *Phys. Rev. Lett.* **2002**, *88*, 057404.
- [14] O. Hildebrand, E. Goebel, K. Romanek, H. Weber, G. Mahler, *Phys. Rev. B* **1978**, *17*, 4775.
- [15] A. Chernikov, C. Ruppert, H. M. Hill, A. F. Rigosi, T. F. Heinz, *Nature Photon.* **2015**, *9*, 466.
- [16] T. B. Arp, D. Pleskot, V. Aji, N. M. Gabor, *Nature Photon.* **2019**, *13*, 245.
- [17] a) M. Amani, D.-H. Lien, D. Kiriya, J. Xiao, A. Azcatl, J. Noh, S. R. Madhupathy, R. Addou, K. Santosh, M. Dubey, *Science* **2015**, *350*, 1065; b) H. Shi, R. Yan, S. Bertolazzi, J. Brivio, B. Gao, A. Kis, D. Jena, H. G. Xing, L. Huang, *ACS Nano* **2013**, *7*, 1072.
- [18] a) D. Sun, Y. Rao, G. A. Reider, G. Chen, Y. You, L. Brézin, A. R. Harutyunyan, T. F. Heinz, *Nano Lett.* **2014**, *14*, 5625; b) Y. Yu, Y. Yu, C. Xu, A. Barrette, K. Gundogdu, L. Cao, *Phys. Rev. B* **2016**, *93*, 201111.
- [19] S. Yuan, R. Roldán, M. Katsnelson, F. Guinea, *Phys. Rev. B* **2014**, *90*, 041402.
- [20] a) H. Wang, C. Zhang, F. Rana, *Nano Lett.* **2014**, *15*, 339; b) H. Wang, C. Zhang, F. Rana, *Nano Lett.* **2015**, *15*, 8204.
- [21] a) T. Korn, S. Heydrich, M. Hirmer, J. Schmutzler, C. Schüller, *Appl. Phys. Lett.* **2011**, *99*, 102109; b) G. Plechinger, A. Castellanos-Gomez, M. Buscema, H. S. van der Zant, G. A. Steele, A. Kuc, T. Heine, C. Schüller, T. Korn, *2D Mater.* **2015**, *2*, 015006.
- [22] a) C. Rice, R. Young, R. Zan, U. Bangert, D. Wolverson, T. Georgiou, R. Jalil, K. Novoselov, *Phys. Rev. B* **2013**, *87*, 081307; b) D. Lloyd, X. Liu, J. W. Christopher, L. Cantley, A. Wadehra, B. L. Kim, B. B. Goldberg, A. K. Swan, J. S. Bunch, *Nano Lett.* **2016**, *16*, 5836.
- [23] Y. Yu, S. Hu, L. Su, L. Huang, Y. Liu, Z. Jin, A. A. Purezky, D. B. Geohegan, K. W. Kim, Y. Zhang, *Nano Lett.* **2014**, *15*, 486.
- [24] A. Gurarlan, Y. Yu, L. Su, Y. Yu, F. Suarez, S. Yao, Y. Zhu, M. Ozturk, Y. Zhang, L. Cao, *ACS Nano* **2014**, *8*, 11522.